Nuclear Instruments and Methods in Physics Research A 804 (2015) 212–220

Contents lists available at ScienceDirect

Nuclear Instruments and Methods in Physics Research A

journal homepage: www.elsevier.com/locate/nima

Preliminary investigation of scintillator materials properties: SrI_2:Eu, $CeBr_3$ and GYGAG:Ce for gamma rays up to 9 MeV

A. Giaz [a,*], G. Hull [b], V. Fossati [c], N. Cherepy [d], F. Camera [a,c], N. Blasi [a], S. Brambilla [a], S. Coelli [a], B. Million [a], S. Riboldi [a,c]

[a] INFN Milano, Via Celoria 16, 20133 Milano, Italy
[b] Institut de Physique Nucleaire d'Orsay, 15 rue Georges Clemenceau, 91406 Orsay Cedex, France
[c] Università degli Studi di Milano, Physics Dept., Via Celoria 16, 20133 Milano, Italy
[d] Lawrence Livermore National Laboratory, Livermore, CA 94550, USA

ARTICLE INFO

Article history:
Received 4 June 2015
Received in revised form
19 August 2015
Accepted 18 September 2015
Available online 30 September 2015

Keywords:
Scitillator detectors;
Gamma raysy;
Gamma Spectroscopy

ABSTRACT

In this work we measured the performance of a $2'' \times 2''$ cylindrical tapered crystal of SrI_2:Eu, a $2'' \times 3''$ cylindrical sample of $CeBr_3$ and a $2'' \times 0.3''$ cylindrical sample of GYGAG:Ce. These scintillators are prototypes in volume or material and were provided by the Lawrence Livermore National Laboratory and by the Institut de Physique Nucléaire d'Orsay. The gamma-ray energy resolution was measured in the energy range of 0.1–9 MeV using different sources. Each scintillator was scanned along *x*, *y* and *z* axes, using a 400 MBq collimated ^{137}Cs source. Owing to the GYGAG:Ce thickness, it was not possible to obtain the value of the energy resolution at 9 MeV and to scan the crystal along the *z* axis. The 662 keV full energy peak position and its FWHM were measured relative to the full energy peaks positions produced by a non-collimated ^{88}Y source. The signals of the detectors were additionally digitized and compared, up to 9 MeV, using a 12 bit LeCroy 600 MHz oscilloscope.

1. Introduction

In the last 10 years several new scintillator materials have been discovered. The lanthanum halides, $LaBr_3$:Ce and $LaCl_3$:Ce, showed excellent performance and are now available in large volumes ($V > 1000\ cm^3$) [1–19]. Small samples (i.e. $1'' \times 1''$) of $CeBr_3$ and SrI_2:Eu crystals appeared a few years later and there is still an intense R&D work on such detectors as the produced volume is constantly increasing over time [20–29]. The development of ceramic scintillator materials offers the possibility to have high-resolution gamma-ray spectroscopy at low cost. Transparent ceramic scintillators, such as GYGAG:Ce, allow gamma-ray spectroscopy performance superior to the most common scintillators [29–34].

For high energy gamma spectroscopy, large volume scintillators are required. We have obtained inch-scale samples of three new scintillators for evaluation of their properties, not yet well-established, for high energy gamma spectroscopy. These scintillator materials have very promising properties, as shown in Table 1. They could be good substitutes for NaI:Tl, the most used scintillator for gamma-ray detection and spectroscopy, as they all offer better energy resolution at 662 keV, higher light yield and higher density. The three studied scintillators could also represent a reasonable alternative for $LaBr_3$:Ce.

SrI_2:Eu has the best energy resolution ($< 3\%$) among the studied detectors, and contains no internal radioactivity, but it is characterized by a slow signal and self-absorption [25–29]. The study of a large volume crystal is then important to understand how much the energy resolution is affected from this phenomenon. Furthermore, while the long decay time constant of SrI_2:Eu could be a critical aspect in case of high-rate experiments, it makes this material a good candidate for being used as a second stage crystal in a phoswich telescope.

$CeBr_3$ is characterized by an energy resolution that is a little worse than that of $LaBr_3$:Ce, but with the convenient advantage of having no internal radioactivity. This could be a good detector for low background experiments and for medical applications, such as PET (position emission tomography), in which a large number of detectors, providing good timing resolution, are involved.

GYGAG:Ce is a transparent ceramic oxide and therefore it is not affected by the problems of the crystal growth. It is neither hygroscopic nor does it contain internal radioactivity and it could be realized potentially in any dimension and shape.

Even though all three scintillator detectors studied in this work could be excellent substitutes of $LaBr_3$:Ce, at the moment, only few

* Corresponding author.
E-mail address: agnese.giaz@mi.infn.it (A. Giaz).

http://dx.doi.org/10.1016/j.nima.2015.09.065
0168-9002/

Table 1
The scintillation properties are compared. The scintillation light yield, the principal emission wavelength, the energy resolution at 662 keV and the density are listed in columns 2, 3, 4 and 5 respectively. The values of the energy resolution in bracket, reported in column 4 are the values measured in this work. As discussed in the text, they are a little bit worse that the expected ones.

Material	Light yield [ph/keV]	Emission [nm]	En. Res. [%]	ρ [g/cm^3]	Ref.
NaI:Tl	38	415	6–7	3.7	[35]
CsI:Tl	52	540	6–7	4.5	[35]
$LaBr_3$:Ce	63	360	3	5.1	[19]
SrI_2:Eu	80	480	3–4 (4)	4.6	[33]
GYGAG:Ce	40	540	<5 (5.2)	5.8	[29–34]
$CeBr_3$	45	370	3.5–4 (4.4)	5.2	[21]

detailed studies on large volume SrI_2:Eu and $CeBr_3$ or in general on GYGAG:Ce scintillators [20–34] are available in literature.

In this work we present the study of the performances of a large diameter ceramic scintillator ($2''\times 0.3''$ GYGAG:Ce) and two large volume new generation scintillator crystals (a SrI_2:Eu $2''\times 2''$ and a $CeBr_3$ $2''\times 3''$). We discuss the dependence of the peak centroid and its FWHM produced using a 1 mm collimated ^{137}Cs source as a function of the position of the interaction point in the detector. Furthermore we compare the anode pulse measured for different gamma-ray energies and for different positions of the collimated source.

This study is focused on the possible use of these crystals for high-energy gamma ray spectroscopy, for which large volume, self-absorption and homogeneity in the light yield are very crucial features.

In Section 2 we describe the measurements performed in the gamma spectroscopy laboratory of the University of Milan. The results obtained for SrI_2:Eu are discussed in Section 3 while those of $CeBr_3$ and GYGAG:Ce in Sections 4 and 5, respectively. For each crystal, we present the results of the energy resolution of the scintillator (Sections 3.1, 4.1, and 5.1), the detector response as a function of the interaction point along the three axes by using a collimated beam of 662 keV gamma rays from a ^{137}Cs source (Sections 3.2, 4.2, and 5.2) and the study of the signal shape up to 9 MeV gamma rays (Sections 3.3, 4.3, and 5.3). Comparison of the properties of these three detectors is given in Section 6, with a conclusion in Section 7.

2. The characterization measurements

This study offers a comparison of three new scintillators, at volumes relevant to high energy gamma spectroscopy applications. The $2''\times 2''$ SrI_2:Eu crystal is among the largest yet produced, the $2''\times 3''$ $CeBr_3$ crystal is one of the biggest available on the market and while the $2''\times 0.3''$ GYGAG:Ce ceramic scintillator is smaller, its performance surpasses other available oxide scintillators. The SrI_2:Eu (3% doped) was grown by RMD while the GYGAG:Ce was produced by Lawrence Livermore National Laboratory (LLNL) which own both samples. The $CeBr_3$ was bought from Scionix and it is from the Institut de Physique Nucléaire d'Orsay. The measurements of the detector performances were carried out in the gamma spectroscopy laboratory of the University of Milan. Table 2 lists the crystals, the PMTs, the voltage dividers (VD) and the voltage applied to the PMTs used for this set of measurements. In the case of $CeBr_3$ two different VDs were used: the first one is a standard VD from HAMAMASTU (E1198-27), while the second one, LABRVD, was developed by the electronic workgroup of the University of Milan and especially designed to work with the $LaBr_3$:Ce scintillators [19,36]. We used this VD (as the $CeBr_3$ signal is very similar to the $LaBr_3$:Ce one) to reduce the PMT induced non linearity in energy. The SrI_2 has been coupled to a larger PMT as no $2''$ PMT were available. This should affect the crystal performances only marginally.

Table 2
Readout configurations used for each scintillator. The scintillators are listed in column 1, the PMTs, voltage dividers and the applied voltages are listed in columns 2, 3, and 4, respectively.

Crystal	PMT	VD	HV (V)
SrI_2	R6233-100SEL	E1198-27	800
GYGAG	R6233-100SEL	E1198-27	850
$CeBr_3$	R6231-100MOD	E1198-27	600
$CeBr_3$	R6231-100MOD	LABRVD	800

The scintillation response was measured using standard gamma ray sources (^{22}Na, ^{60}Co, ^{88}Y, ^{133}Ba, ^{137}Cs, ^{152}Eu) and an AmBe(Ni) composite source for gamma rays up to 9 MeV [37]. In the latter, a core of ^{9}Be and alpha-unstable ^{241}Am is surrounded by a thick layer of paraffin; some metal discs of nickel are also placed inside the paraffin layer. When an alpha particle is emitted by the ^{241}Am, there is a high probability that it is captured by ^{9}Be, leading to ^{9}Be(α,n)^{12}C reaction. The neutrons are thermalized by multiple scattering in the paraffin layer, which serves both as moderator and as shielding.

The signals of the three detectors were sent to a spectroscopic amplifier (TENNELEC TC244) and to an ADC (ORTEC ASPEC MCA 926). The detector anode pulses were also digitized using a 12 bit LeCroy HDO 6054 oscilloscope. A set of pulses ($\sim$1000) at a fixed energy were averaged to produce the reference signals. The signal properties (rise time and fall time) of all detectors were compared and the signals of each scintillator were studied from 662 keV up to 9 MeV. The rise time and the fall time are the convolution between the detector signal and the PMT intrinsic response.

The energy spectra and the pulses were measured using a collimated beam of 662 keV gamma rays scanning the detector along the x, y, and z axes.

A non-collimated ^{88}Y source, providing two calibration points, was placed nearby and used as a reference. In this way it was possible to study how the position of the centroid, the FWHM, and the area of the peak at 662 keV changes as a function of the position of the incident radiation. The set-up, shown in Fig. 1, was composed of the detector under test, a collimated source of 400 MBq of ^{137}Cs and a platform which could be moved both along the x and the y axes by adjusting a micrometer screw. The collimator of heavy metal [38] was 8 cm long with a hole diameter of 1 mm, so that 96% of the γ rays were collimated within a 1 mm wide beam spot. The detector was placed on a second platform that is maintained at a fixed position. The source was placed in front of the detector by hands and the two platforms were aligned by eye. Particular care was taken to place the gamma ray beam perpendicular to the detector. The distance between the detector surface and the collimator was about 1.5 cm.

2.1. Test limitations

As previously discussed the signals of the three detectors were sent to a spectroscopic amplifier (TENNELEC TC244) and to an ADC (ORTEC ASPEC MCA 926) or, alternatively, the detector anode pulses were digitized using a 12 bit LeCroy HDO 6054 oscilloscope. The aim of this work was, in fact, to test these detector's performances using a standard electronics chain. The energy resolution measured using such approach could not be the 'best achievable' as will be discussed for the different detectors, therefore it is important to remember that (i) The SrI2:Eu is not tested using a digital readout which should be able to overcome effects of self-

absorption and re-emission (see discussion in Section 3) (ii) CeBr3 is tested with an "issue" substantially worsening its energy resolution as it was the retreated by scionix (see discussion in Section 4), (iii) GYGAG:Ce readout does not offer sufficient quantum efficiency and the crystal is too thin for an efficient high energy gamma-ray detection.

3. The SrI_2:Eu scintillator

3.1. The energy resolution

The energy resolution of the SrI_2:Eu crystal was studied using standard gamma sources (^{152}Eu, ^{137}Cs, ^{60}Co, ^{88}Y) and an AmBe(Ni) composite source. The detector was placed on the paraffin over the AmBe source. The spectra using the other sources was measured placing them in front of the crystal but not necessary on the crystal axis. The used detector–source distance was chosen to have a count rate of approximately 1 kHz. The signal of the detector was sent to the amplifier (TENNELEC TC 244). The shaping time was set to 12 μs.

Fig. 2 shows the energy spectrum obtained by irradiating the scintillator with a ^{137}Cs and a ^{60}Co source. The measured energy resolution is ~4.0% at 662 keV (FWHM~27 keV). The possibility to have different sources allows to measure the trend of the energy resolution. Fig. 3 shows the energy resolution trend as a function of the gamma-ray energy. The continuous line, in Fig. 3 represents the expected trend ($R \propto 1/\sqrt{E}$). Since the 4.4 MeV peak FWHM has an intrinsic width, as explained in Section 2, it could not be used for the energy resolution trend. The 9 MeV peak FWHM (see Fig. 4) was estimated to be 100 ± 20 keV (1.1%) which is consistent with the expected trend.

The energy spectra of the crystal were obtained via two methods: in the first case we used the TENNELEC amplifier, while in the second one we obtained the spectra from the digitized signals. The measured energy resolution are comparable with the two methods.

The energy resolution obtained with the same crystal and other large volume SrI_2:Eu crystals at Lawrence Livermore Laboratory, using instead the digital readout method, was better than 3% [31,33] and this is consistent with what we have found using the collimated gamma rays source (see Section 3.2). With the digital readout, an on-the-fly correction factor is applied to the scintillation pulses as a function of their effective decay time, thus accounting for self-absorption and allowing and accurate energy histogram (gamma spectrum) to be obtained [31,33].

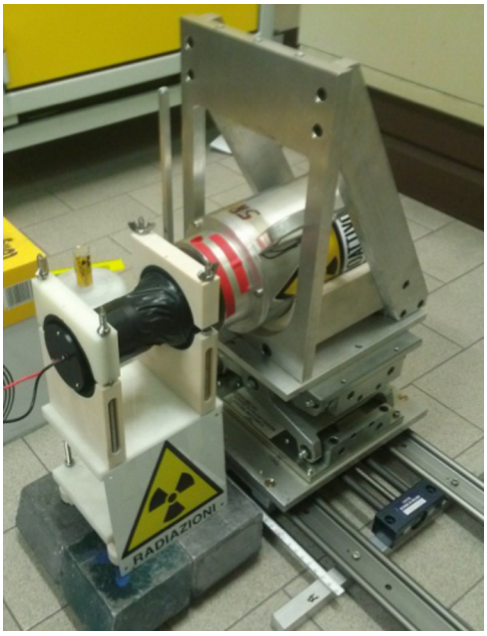

Fig. 1. The set-up used to study the detector response as a function of the interaction point. The source is on a platform that could be moved both along the *x* and the *y* axes with a micrometer screw.

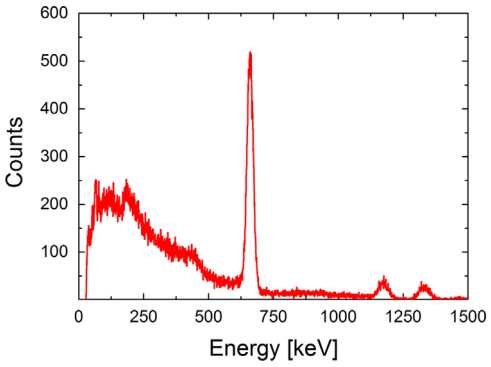

Fig. 2. The energy spectrum of the SrI_2:Eu scintillator, acquired with a standard spectroscopic chain, using 12 μs of shaping time. The sources were ^{60}Co and ^{137}Cs. The energy resolution is about 4% at 662 keV. The acquisition time was about 10 min.

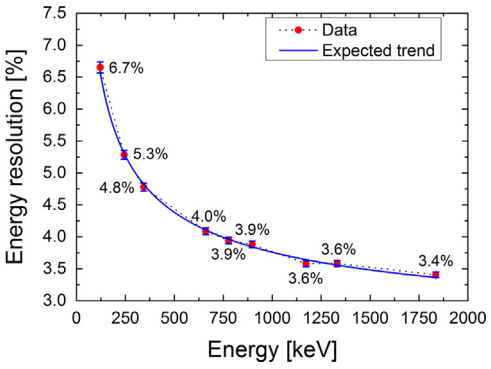

Fig. 3. The measured energy resolution as a function of the energy of the incident radiation. The continuous line indicates the expected trend ($E \propto 1/\sqrt{E}$).

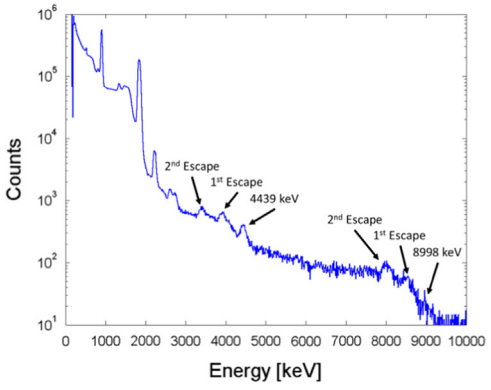

Fig. 4. The energy spectrum of the SrI_2:Eu, acquired with a standard spectroscopic amplifier and ADC. The sources used were ^{88}Y and AmBe(Ni). The acquisition time was about 6 h.

3.2. Detector response as a function of the interaction point

The detector response as a function of the interaction position was studied along the crystal axes. We chose the *x* and *y* axes, on the crystal face. The *z* axis was the cylindrical symmetry axis, starting from the PMT to the crystal frontal face, as shown in Fig. 5.

To measure the detector response as a function of the interaction point, it is important to point out that the SrI_2:Eu is 2" × 2" cylindrical tapered and its volume is 51.6 cm^3. The difference from a 2" × 2" is smaller than few millimeters on the front face (diameter front face 4.9 cm and diameter of back face is 5.1 cm). The collimated source of ^{137}Cs was placed on a platform and moved with a micrometric screw. The measured energy spectra were calibrated using the ^{88}Y source. The position of the centroid with respect to the ^{88}Y peaks, the FWHM and the area of the 662 keV gamma peak were studied. The acquisition rate was 400 Hz.

The position of the centroid shows a variation of ~3%, moving the source along the *x* and the *y* axes. Based on previous studies, we believe this to be due to optical "light-trapping" resulting from the Eu^{2+} self-absorption and re-emission [27]. Along lateral surfaces we also observe small variations of the centroid position (those are included in the ~3%, mention above), FWHM, owing to absorption phenomena.

Figs. 6 and 7 show the full energy peak and its FWHM as a function of the interaction position along the *z* axis. The energy resolution changes from 22 keV (3.2%) up to 34 keV (5.1%).

The result of the self-absorption effect is that a digital readout method, described by Cherepy and co-authors is needed to obtain the best possible energy resolution with large volume crystals [31,33]. The digital readout method was explained in Section 3.1.

3.3. Signal shape

The signal shape of the SrI_2:Eu was studied from 662 keV up to 9 MeV. The signals of the detector were digitized with a LeCroy waverunner oscilloscope (HDO 6054). The sampling frequency was 0.5 Gsamples/s and the sampling range was 20 μs.

A set of pulses (~1000) were average to produce the pulses of Fig. 8. At 9 MeV, the signals, whose energy is in a range of 1 MeV (from 8 MeV up to 9 MeV), were used to produce the average signal (see legend of Fig. 8). The rise time (10–90% of amplitude) was calculated for all the averaged signals and it was found equal to 24 ± 2 ns. No rise time variations were observed as a function of the energy of the incident gamma ray. The fall time (90–10% of amplitude) of the average signals was measured to be 7 μs. Fig. 8 shows the average signals of the SrI_2:Eu. The plot shows that at different deposited energies no significant changes in pulse shape is observed, therefore only one curve is practically observable in Fig. 8.

The signal shape was also studied as a function of the gamma-ray interaction point along the *z* axis (*z*=0.5 cm is the measured point closest to the PMT). Four different positions along the *z* axis

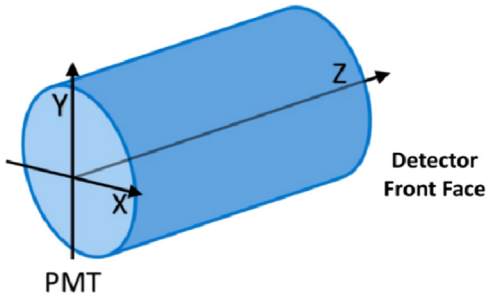

Fig. 5. The coordinate system used for the measurements of the detectors' response as a function of the interaction point.

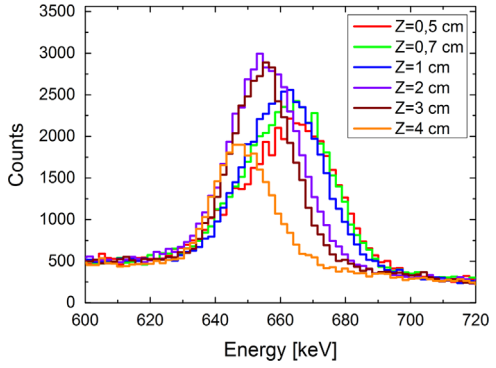

Fig. 6. The 662 keV peaks from a collimated ^{137}Cs source on the SrI_2:Eu crystal. The different peaks were acquired by moving the collimated beam along the *z* axis of the crystal, where *z*=0 is at the PMT window. The spectra were calibrated using a non-collimated ^{88}Y sources that was placed nearby as a reference.

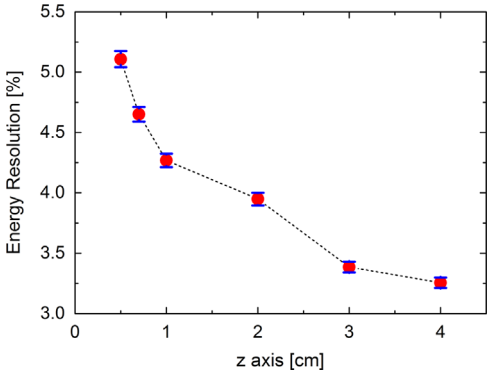

Fig. 7. The FWHM of 662 keV peaks from a collimated ^{137}Cs source on the SrI_2:Eu crystal. The different values were obtained by moving the collimated beam along the *z* axis of the crystal. The origin of the *z* axis is the PMT side, as shown in Fig. 5. The spectra were calibrated using a non-collimated ^{88}Y sources that was placed nearby as a reference.

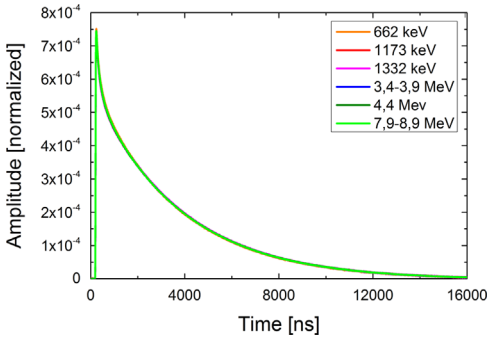

Fig. 8. The area normalized average pulses of the SrI_2:Eu excited gamma rays from 662 keV up to 9 MeV. No significant changes in shape are present. The areas of the pulses are normalized to one. The different curves overlap and therefore only one line is visible.

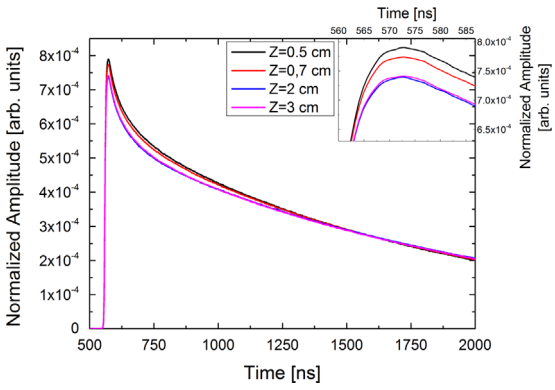

Fig. 9. The area normalized pulses of the SrI_2:Eu for the 662 keV gamma ray from a collimated ^{137}Cs source. The area of the pulses is normalized to one.

were selected, as shown in Fig. 9. The signals are different as a function of the interaction point, as it is emphasized in the inset of Fig. 9. The rise time remains unchanged while the fall time is longer (it changes from 6.7 μs to 7.3 μs) when gamma rays enter near the PMT. The area of the pulses is normalized to one to underline the different shapes shown in Fig. 9.

4. The $CeBr_3$ scintillator

4.1. The energy resolution

The signal of the $CeBr_3$ detector was sent to a spectroscopy amplifier (TC 244) and the shaping time was set to 1 μs.

Fig. 10 shows the energy spectra acquired when irradiating the scintillator with ^{88}Y, ^{60}Co and AmBe(Ni) radioactive sources. The measured energy resolution is $4.4 \pm 0.1\%$ at 662 keV (FWHM$\sim$29 keV). As for the SrI_2 the measured energy resolution follows the expected trend ($R \propto 1/\sqrt{E}$). The measured FWHM for the 9 MeV gamma-rays is 120 ± 5 keV which is comparable with the expected value of 108 keV. The 9 MeV peak, in bottom panel of Fig. 6, is located at 8.6 MeV due to the non-linearity of the PMT tube ($\sim$4% at 9 MeV). To reduce the non-linearity effect we coupled the PMT to an active voltage divider especially designed for the $LaBr_3$:Ce detectors, called LABRVD [19,36]. The energy resolution was unchanged but the measured non linearity reduced to 1%.

The measured energy resolution for this detector is bigger than the nominal value (3.6% at 662 keV) due to an issue in the crystal gluing process repaired after these tests. At present, after a repair procedure performed by the crystal manufacturer the detection properties of the scintillators are completely recovered. The measured value of the energy resolution does not affect the detector response as a function of the interaction point (Section 4.2) and the signal properties (Section 4.3).

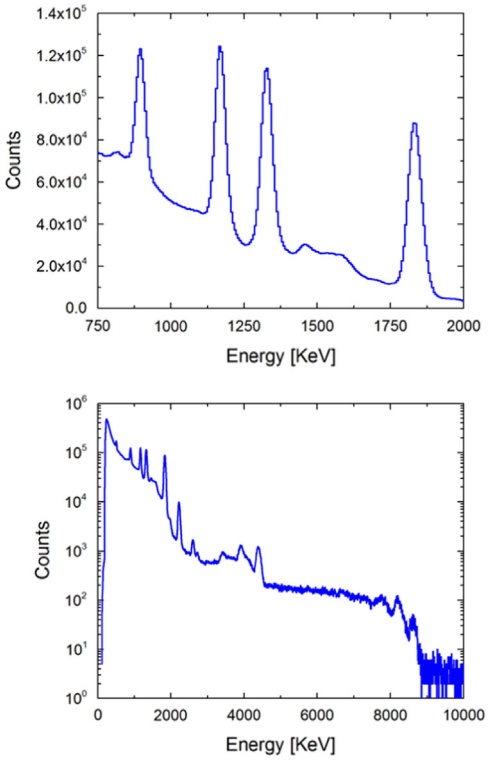

Fig. 10. The energy spectrum of the $CeBr_3$, acquired with a standard spectroscopic amplifier and ADC. The sources used were ^{60}Co and ^{88}Y and AmBe(Ni). Top panel: zoom of the low-energy part of the spectrum. Bottom panel: the whole energy spectrum. The acquisition time was about 16 h.

4.2. Detector response as a function of the interaction point

Fast The detector response as a function of the interaction point was studied along the crystal axes, as done for the SrI_2:Eu (Section 3.2). In this case, the acquisition rate was 1000 Hz, due to the acquisition threshold that was very low.

The position of the centroid as well as the peak FWHM and area, does not show variations while moving the source along the x and the y axes. The x-y scans confirm the fact that the loss of light yield was uniform across the optical window. Fig. 11 shows the peak at 662 keV for different interaction positions along the z axis and in this case a variation of the centroid position and width is visible. The energy resolution remains however constant around 28–29 keV at 662 keV (4.4%), as shown in Fig. 12.

4.3. Signal shape

The anode signal line-shape was studied from 662 keV up to 9 MeV. The only difference with respect to the SrI_2:Eu measurement was in the sampling frequency of the signal (2.5 Gsamples/s), owing to the fast $CeBr_3$ signal. A constant rise time of 18 ns (10–90% of amplitude) was extracted for all signals. The fall time of the signals is about 70 ns.

Fig. 13 shows the averaged signals for different energies. The small observed changes in the signal line-shape could be explained by a non-linearity effect in the PMT, owing to the fast

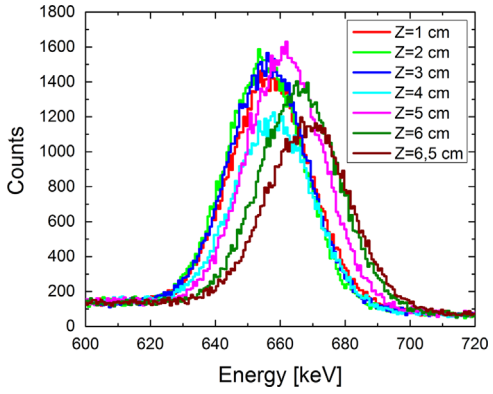

Fig. 11. The 662 keV peaks from a collimated ^{137}Cs source on the $CeBr_3$ crystal. The different peaks were acquired by moving the collimated beam along the z axis of the crystal. The spectra were calibrated using a non-collimated ^{88}Y sources that was placed nearby as a reference.

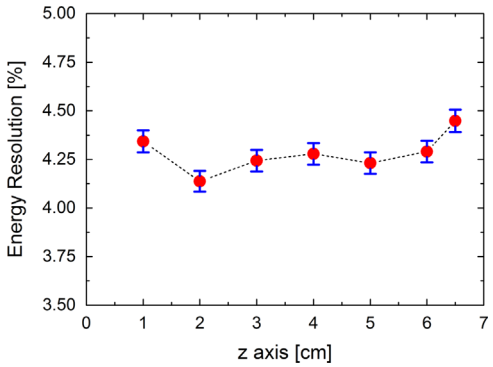

Fig. 12. The FWHM of 662 keV peaks from a collimated ^{137}Cs source on the $CeBr_3$ crystal. The different values were obtained by moving the collimated beam along the z axis of the crystal. The origin of the z axis is the PMT side, as shown in Fig. 5.

signal and high light yield of $CeBr_3$. A similar non-linearity effect was already observed for $LaBr_3$:Ce [19].

5. The GYGAG:Ce scintillator

5.1. The energy resolution

The GYGAG:Ce ceramic scintillator, differently from the previous two materials, is neither a single crystal nor hygroscopic. Therefore, it was directly coupled to the PMT (HAMAMATSU R6233-100sel). The scintillator was covered by Teflon to optimize the light collection and the energy resolution.

The energy resolution of the GYGAG:Ce scintillator was studied using standard gamma-emitting sources (^{152}Eu, ^{137}Cs, ^{60}Co, ^{88}Y), as for the other two crystals. The ceramic was coupled to a HAMAMATSU R6233-100sel PMT. The shaping time of the amplifier was set to 6 μs. As for the previous two detectors the measured energy resolution values follow the expected trend ($R \propto 1/\sqrt{E}$).

Fig. 14 shows the energy spectrum acquired irradiating the scintillator with a ^{137}Cs and a ^{60}Co source at the same time. The measured energy resolution is $5.2 \pm 0.1\%$ at 662 keV (FWHM ~34 keV). The used PMT is equipped with a photocathode optimized for the blue region of visible spectrum while for the GYGAG:Ce, typical emission wave-length is in the yellow (530 nm). Thus, the quantum efficiency of the used PMT, which is about 35% at 350 nm, is considerably reduced (around 12%) at 530 nm. If using a device with a quantum efficiency of ~35% in the yellow region, we expect an energy resolution of ~3.2% at 662 keV. Furthermore the energy resolution of the GYGAG:Ce could be also affected by the afterglow phenomenon. To limit and eventually eliminate this effect, it is necessary to store GYGAG:Ce (after handling in room lights) in the dark for several days before using, to obtain the best possible energy resolution. This same scintillator, measured in [34] offered 4.9% resolution at 662 keV. The measurements reported here were performed 48 h after coupling the ceramic with the PMT and wrapping it with black tape for light tightness. The value of the energy resolution does not significantly affect the detector response as a function of the interaction point (Section 5.2) and the signal properties (Section 5.3). The energy resolution of the smaller ceramic samples was $<4\%$ with a silicon photodiode, in optimized condition at LLNL [34].

High-energy gamma rays from the AmBe(Ni) source were measured also using the GYGAG:Ce detector. However, the peak at 9 MeV is just barely visible, as shown in Fig. 18, due to the low statistics accumulated due to the reduced thickness of the detector.

5.2. Detector response as a function of the interaction point

The detector response as a function of the interaction point was studied along the crystal axes, using for the GYGAG:Ce the same experimental procedure, already described for the other scintillators. Owing to the crystal thickness (0.3″), the response was studied only along the *x* and *y* axes. In this case, the acquisition rate was 800 Hz.

The position of the centroid does not show variations. Furthermore the FWHM and area are constant (the variation is smaller than 10%), as well. Fig. 15 shows the trend of the FWHM as

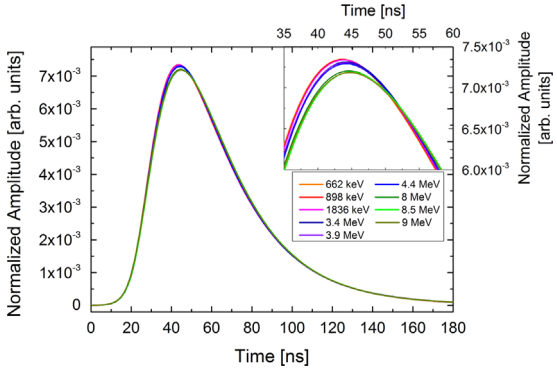

Fig. 13. The area normalized average pulses of the $CeBr_3$ for gamma rays from 662 keV up to 9 MeV. Changes in shape are present, as shown in the inset. These changes are related on the PMT non-ideal behavior owing to the high light yield and the fast signal (rise time ~20 ns and fall time ~70 ns) of $CeBr_3$.

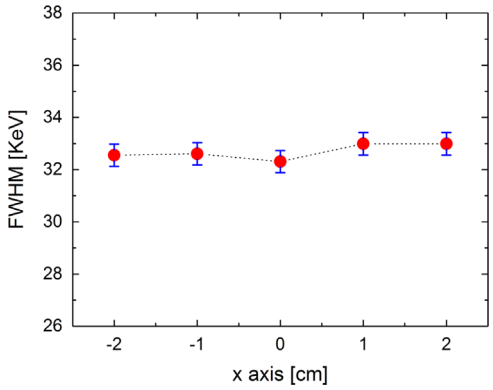

Fig. 15. The FWHM of 662 keV peaks from a collimated ^{137}Cs source on the GYGAG:Ce scintillator. The different values were obtained by moving the collimated beam along the *x* axis of the crystal. The spectra were calibrated using a non-collimated ^{88}Y sources that was placed nearby as a reference.

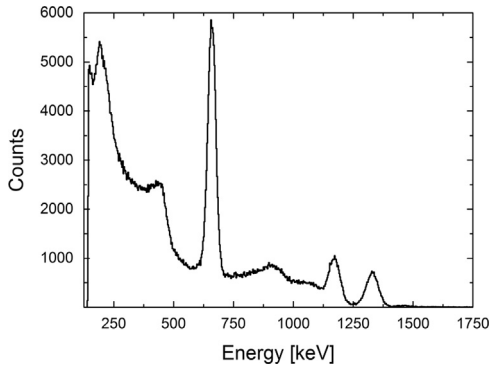

Fig. 14. The energy spectrum of the GYGAG:Ce, acquired by standard spectroscopic amplifier and an ADC. The sources used were ^{60}Co and ^{137}Cs. The acquisition time was about 1 h.

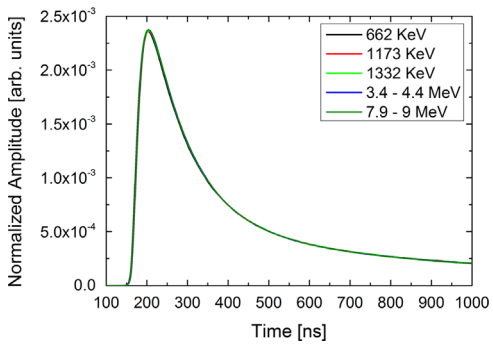

Fig. 16. The area normalized average pulses of the GYGAG:Ce for the 662 keV gamma ray from a collimated ^{137}Cs source. No significant changes in shape are present.

a function of the interaction position along the x axis. The FWHM value is almost constant about 33 keV at 662 keV ($<$ 5%).

5.3. Signal line-shape

In this section, the signal shape of the GYGAG:Ce was studied from 662 keV up to 9 MeV. The sampling frequency was 1.25 G samples/s. As at 4 MeV and at 9 MeV the statistic was not high, a range of 1 MeV (from 3.5 MeV up to 4.5 MeV and from 8 MeV up to 9 MeV, respectively) was used to select the signals.

The signal of the GYGAG:Ce has a rise time (10–90% of amplitude) of 26 ns. The PMT (HAMAMATSU R6233-100sel) intrinsic rise time that is 9.5 ns at 1000 V, could affect this value. The fall time of the average signals is about 700 ns.

Fig. 16 shows the average signals for the different investigated gamma-ray energies. No significant changes in shape were observed neither changing gamma-ray energy nor the incident position of the 662 keV collimated source.

6. Detector Comparison

The detectors that have been studied in this work, SrI_2:Eu, $CeBr_3$:Ce and GYGAG:Ce scintillators show energy resolution of 4.0%, 4.4% and 5.2% at 662 keV, respectively. All the values of the energy resolution are better than that of NaI:Tl (6% at 662 keV), the most widely used scintillator for gamma spectroscopy. The spectra measured using an ^{152}Eu source are compared in Fig. 17.

The energy spectra acquired irradiating the scintillators under test with an AmBe(Ni) source, which provides gamma rays up to 9 MeV, are compared in Fig. 18. The $CeBr_3$ spectrum shows clearly the 9 MeV peak and the corresponding first and second escape peaks. $CeBr_3$ has the largest volume ($2'' \times 3''$) and has a density of 5.2 g/cm^3. Because of the reduced statistics, the 9 MeV peak, its first escape and its second escape peaks are observed with SrI_2, though not as clearly as for $CeBr_3$. The thickness of the GYGAG:Ce is 0.3″ and therefore the 9 MeV peak is barely visible. It is important to point out that the spectra of Fig. 18 are normalized to the area of the 898 keV peak of the ^{88}Y source.

The signals of the three detectors for energies ranging between 662 keV and 9 MeV were digitized and compared. Fig. 19 shows the comparison of the three signal shapes, at 662 keV, for the three scintillators. The $CeBr_3$ provides the fastest signal: it has a rise time of ~18 ns and a fall time of ~70 ns. Otherwise SrI_2:Eu has the slowest signal among the tested detectors (fall time ~7 μs).

The detector response as a function of the interaction point is almost constant for the $CeBr_3$ and the GYGAG:Ce, in which no

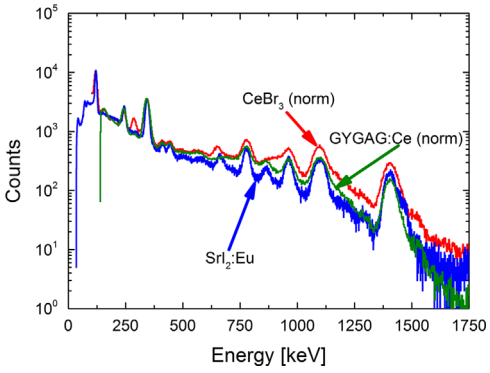

Fig. 17. The ^{152}Eu energy spectra acquired using a standard spectroscopic amplifier for the three tested scintillators. The SrI_2:Eu has the best energy resolution among these scintillators. The spectra are normalized on the area of the 344 keV peak of the ^{152}Eu source. The presence of an AmBe source near the $CeBr_3$ detector could be the oring of the peak at 295 keV.

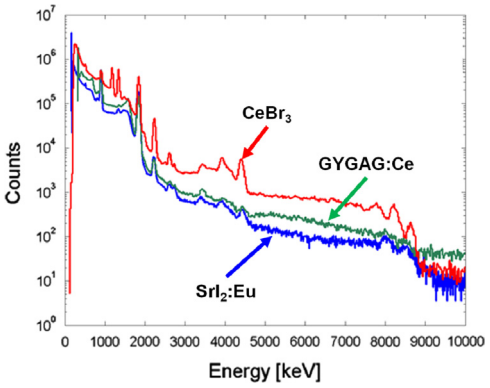

Fig. 18. The measured SrI_2:Eu, GYGAG:Ce and $CeBr_3$ acquired using a standard spectroscopic amplifier and an ADC. The used sources were AmBe(Ni) and ^{88}Y. The $CeBr_3$ spectrum shows also the two ^{60}Co peaks and it is the detector with highest statistics at 9 MeV owing to its large volume and to a long the acquisition time (6, 4, and 16 h for the SrI_2:Eu, the CeBr3 and the GYGAG:Ce, respectively). The spectra are normalized to the area of the 898 keV peak of the ^{88}Y source.

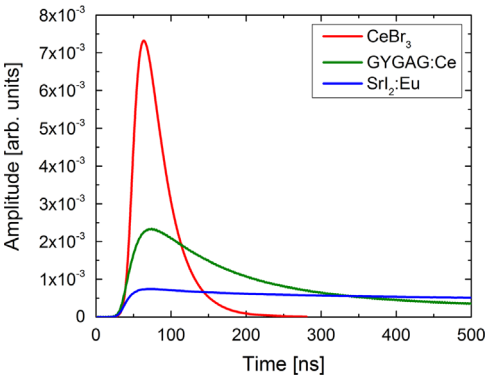

Fig. 19. The area normalized pulses of the three detectors for 662 keV gamma rays. The $CeBr_3$ has the fastest signal among these scintillators (similar to that of $LaBr_3$:Ce), whereas SrI_2:Eu has the slowest signal.

significant variation of the peak position or the FWHM are observed. While SrI_2:Eu detector shows variations in the FWHM along the z axis imputable to the self-absorption effect.

SrI_2:Eu has the best energy resolution among the studied detectors (4.0% at 662 keV), but this value depends on the position of the gamma-ray interaction point. Self-absorption affects the energy resolution of this detector. A FWHM value as good as 22 keV at 662 keV (3.3%), measured with the collimated source. This crystal has a slow decay time constant and so for this reason it would not be suited to high-rate experiments, nevertheless this scintillator can find a possible application as a second stage crystal in a phoswich detector, or for low count rate applications such as environmental monitoring, as it also has no intrinsic radioactivity.

$CeBr_3$ has an energy resolution (the measured value is 4.4% at 662 keV) that is a little worse than that of $LaBr_3$:Ce, but it is still considerably better than NaI:Tl. The absence of internal activity make this crystal ideal for low background measurements or in the cases in which an array with several detectors is used. The detector is characterized by a fast signal, similar to $LaBr_3$:Ce, therefore it could be used successfully in the case of high counting rate. The energy resolution is expected to be better (about 3%) at 662 keV in the case of co-doped crystal [20] but, at present co-doped $CeBr_3$ is still not commercially available. We observed non linearity effects at 9 MeV, as is also typically observed with $LaBr_3$:Ce scintillators. No significant variation of the peak centroid the FWHM or of the area were observed as a function of the interaction point.

GYGAG:Ce provides high efficiency and good energy resolution of 5% at 662 keV with a PMT equipped with a non-optimal

photocathode (blue sensitive, rather than green/yellow sensitive to match the 500–650 nm emission). No variations of the peak centroid, the FWHM or the area are observed as a function of the interaction point, along the x and the y axes.

7. Conclusion

In this work relatively large volume SrI_2:Eu, $CeBr_3$:Ce and GYGAG:Ce scintillators were characterized by studying the pulse shape, the energy resolution their response to a collimated source and to 9 MeV γ-rays. All three scintillators offer improved energy resolution, compared to standard scintillators, such as NaI:Tl.

The detector sizes (6 in^3 SrI_2:Eu, 9 in^3 $CeBr_3$ and 1 in^3 GYGAG:Ce scintillators) are large enough in volume to measure medium/high energy gamma rays and assess the homogeneity of their response. SrI_2:Eu, shows the best energy resolution, however self-absorption impairs the performance when standard analog readout is used (as reported here). The SrI_2:Eu is an excellent candidate for applications in which small volumes are used. The energy resolution for large volume SrI_2:Eu can match that of small crystals ($<3\%$ at 662 keV) only if digital readout methods (capable to nullify self absorption effects) are applied, though the resolution obtained here with analog readout, R(662 keV), 4% is still better than NaI:Tl. It is free of intrinsic radioactivity and its relatively slow decay time is still fast enough to applications to measure low count rate sources.

$CeBr_3$ is 100% Ce doped $LaBr_3$:Ce, thus it is without internal radiation, but suffers from slightly worse energy resolution. Its fast decay time is useful in high count rate applications. It can be used to measure high energy γ-rays with good energy resolution and we have measured 1.1% at 9 MeV. As it is not doped very large volume crystals are not found to suffer from inhomogeneity.

The GYGAG:Ce seems to be an excellent detector without intrinsic radioactivity, while providing high efficiency and good energy resolution. Furthermore, the ceramic detectors offer the attractive possibility to be produced in any shape or dimension, and to be more stable to mechanical shock and to not degrade in humid conditions than halide single crystals. However, GYGAG:Ce ceramics, are not yet commercially available.

Acknowledgments

We would like to acknowledge Rastgo Hawrami and RMD Inc. for growing the SrI_2:Eu crystal, Patrick Beck (LLNL) for characterizing it after encapsulation at LLNL, and Zachary Seeley (LLNL) for fabrication of the GYGAG:Ce ceramic. The LLNL effort was performed under the auspices of the U.S. DOE by Lawrence Livermore National Laboratory under Contract DE-AC52-07NA27344, and has been supported by the US Department of Homeland Security, Domestic Nuclear Detection Office, under competitively awarded IAA HSHQDC-12-X-00149, and the US DOE National Nuclear Security Administration, Defense Nuclear Nonproliferation Research and Development under Contract no. DE-AC03-76SF00098. This support does not constitute an express or implied endorsement on the part of the Government.

This work was also supported by *NuPNET-ERA-NET* within the theNuPNET GANAS project, under Grant agreement no. 202914 and from the European Union, within the "7th Framework Program" FP7/2007-2013, under Grant agreement no. 262010 – ENSAR-INDESYS.

References

[1] BrilLanCescintillatorsperformancesummary.pdf ⟨http://www.detectors.saint-go bain.com/Brillance380.aspx⟩.
[2] E.V.D. Van Loef, P. Dorenbos, C.W.E. van Eijk, K. Kramer, H.U. Gudel, Applied Physics Letters 79 (10) (2001) 1573.
[3] E.V.D. Van Loef, P. Dorenbos, C.W.E. van Eijk, K. Kramer, H.U. Gudel., Nuclear Instruments and Methods in Physics Research Section A 486 (1–2) (2002) 254.
[4] W.W. Moses, Nuclear Instruments and Methods in Physics Research Section A 487 (1–2) (2002) 123.
[5] P. Dorenbos, J.T.M. de Hass, C.W.E. Eijk, IEEE Transactions on Nuclear Science NS51 (3) (2004) 1289.
[6] B.D. Milbrath, J.I. McIntyre, R.C. Runkle, L.E. Smith, IEEE Transactions on Nuclear Science NS53 (5) (2006) 3031.
[7] A. Iltis, M.R. Mayhugh, P. Menge, C.M. Rozsa, O. Selles, V. Solovyev, Nuclear Instruments and Methods in Physics Research Section A 563 (2) (2006) 359.
[8] M. Moszynski, M. Gierlik, M. Kapusta, A. Nassalski, T. Szczęśniak, Ch Fontaine, P. Lavoute, Nuclear Instruments and Methods in Physics Research Section A 567 (1) (2006) 31.
[9] M. Moszynski, A. Nassalski, A. Syntfeld-Każuch, T. Szczęśniak, W. Czarnacki, D. Wolski, G. Pausch, J. Stein, Nuclear Instruments and Methods in Physics Research Section A 568 (2) (2006) 739.
[10] S. Normand, A. Iltis, F. Bernard, T. Domenech, P. Delacour, Nuclear Instruments and Methods in Physics Research Section A 572 (2) (2007) 754.
[11] A. Owens, A.J.J. Bos, S. Brandenburg, E.-J. Buis, C. Dathy, P. Dorenbos, C.W.E. van Eijk, S. Kraft, R.W. Ostendorf, V. Ouspenski, F. Quarati, Nuclear Instruments and Method in Physics Research Section A 572 (2) (2007) 785.
[12] F. Quarati, A.J.J. Bos, S. Brandenburg, C. Dathy, P. Dorenbos, S. Kraft, R. W. Ostendorf, V. Ouspenski, A. Owens, Nuclear Instruments and Method in Physics Research Section A 574 (1) (2007) 115.
[13] P. Menge, G. Gautier, A. Iltis, C. Rozsa, V. Solovyev, Nuclear Instruments and Method in Physics Research Section A 579 (1) (2007) 6.
[14] R. Nicolini, F. Camera, N. Blasi, S. Brambilla, R. Bassini, C. Boiano, A. Bracco, F.C. L. Crespi, O. Wieland, G. Benzoni, S. Leoni, B. Million, D. Montanari, A. Zalite, Nuclear Instruments and Method in Physics Research Section A 582 (2) (2007) 554.
[15] F.C.L. Crespi, F. Camera, N. Blasi, A. Bracco, S. Brambilla, B. Million, R. Nicolini, L. Pellegri, S. Riboldi, M. Sassi, O. Wieland, F. Quarati, A. Owens, Nuclear Instruments and Method in Physics Research Section A 602 (2) (2009) 520.
[16] M. Ciemala, D. Balabanski, M. Csatlós, J.M. Daugas, G. Georgiev, J. Gulyás, M. Kmiecik, A. Krasznahorkay, S. Lalkovski, A. Lefebvre-Schuhl, R. Lozeva, A. Maj, A. Vitez, Nuclear Instruments and Method in Physics Research Section A 608 (1) (2009) 76.
[17] M. Nocente, M. Tardocchi, I. Chugunov, R.C. Pereira, T. Edlington, A. M. Fernandes, D. Gin, G. Grosso, V. Kiptily, A. Murari, A. Neto, E. Perelli Cippo, A. Pietropaolo, I. Proverbio, A. Shevelev, J. Sousa, B. Syme, G. Gorini, J.E.T.-E.F.D. A. Contributors, Review of Scientific Instruments 81 (10) (2010) 10D321.
[18] M. Nocente, M. Tardocchi, A. Olariu, S. Olariu, R.C. Pereira, I.N. Chugunov, A. Fernandes, D.B. Gin, G. Grosso, V.G. Kiptily, A. Neto, A.E. Shevelev, M. Silva, J. Sousa, G. Gorini, IEEE Transactions on Nuclear Science NS60 (2) (2013) 1408.
[19] A. Giaz, L. Pellegri, S. Riboldi, F. Camera, N. Blasi, C. Boiano, A. Bracco, S. Brambilla, S. Ceruti, S. Coelli, F.C.L. Crespi, M. Csatlòs, S. Frega, J. Gulyàs, A. Krasznahorkay, S. Lodetti, B. Million, A. Owens, F. Quarati, L. Stuhl, O. Wieland, Nuclear Instruments and Method in Physics Research Section A 729 (1) (2013) 910.
[20] F. Quarati, M.S. Alekhin, K.W. Krämer, P. Dorenbos, Nuclear Instruments and Method in Physics Research Section A 735 (1) (2014) 655.
[21] F. Quarati, P. Dorenbos, J. van der Biezen, A. Owens, M. Selle, L. Parthier, P. Schotanus, Nuclear Instruments and Method A 729 (1) (2013) 596.
[22] P. Guss, M. Reed, D. Yuan, A. Reed, S. Mukhopadhyay, Nuclear Instruments and Method in Physics Research Section A 608 (2) (2009) 297.
[23] W. Drozdowski, P. Dorenbos, A.J.J. Bos, G. Bizarri, A. Owens, F.G.A. Quarati, IEEE Transactions on Nuclear Science NS55 (3) (2008) 1391.
[24] K. Shah, J. Glodo, W. Higgins, E. van Loef, W.W. Moses, S.E. Derenzo, M. J. Weber, IEEE Transactions on Nuclear Science NS52 (6) (2005) 1391.
[25] N. Cherepy, S.A. Payne, B.W. Sturm, O.B. Drury, S.P. O'Neal, P.A. Thelin, K. S. Shah, R. Hawrami, M. Momayezi, B. Hurst, A. Burger, B. Wiggins, P. Bhattacharya, L.A. Boatner, J.O. Ramey, IEEE Transactions on Nuclear Science NS60 (2) (2013) 955.
[26] P. Belli, R. Bernabei, R. Cerulli, F.A. Danevich, E. Galenin, A. Gektin, A. Incicchitti, V. Isaienko, V.V. Kobychev, M. Laubenstein, S.S. Nagorny, R. B. Podviyanuk, S. Tkachenko, V.I. Tretyak, Nuclear Instruments and Method in Physics Research Section A 670 (1) (2012) 10.
[27] B.W. Sturm, N.J. Cherepy, O.B. Drury, P.A. Thelin, S.E. Fisher, S.A. Payne, A. Burger, L.A. Boatner, J.O. Ramey, K.S. Shah, R. Hawrami, Nuclear Instruments and Method in Physics Research Section A 652 (1) (2011) 242.
[28] J. Glodo, E.V. Van Loef, N.J. Cherepy, S.A. Payne, K.S. Shah, IEEE Transactions on Nuclear Science NS57 (3) (2010) 1228.
[29] N. Cherepy, S.A. Payne, B.W. Sturm, J.D. Kuntz, Z.M. Seeley, B.L. Rupert, R.D. Sanner, O.B. Drury, T.A. Hurst, S.E. Fisher, M. Groza, L. Matei, A. Burger, R. Hawrami, K.S. Shah, L.A. Boatner, Comparative gamma spectroscopy with SrI2 (Eu), GYGAG(Ce) and bi-loaded plastic scintillators in: Proceedings of the Nuclear Science Symposium Conference Record (NSS/MIC), 2010, p. 1288.
[30] Z. Seeley, N.J. Cherepy, S.A. Payne, Journal of Crystal Growth 379 (1) (2013) 79.
[31] N. Cherepy, Z.M. Seeley, S.A. Payne, P.R. Beck, O.B. Drury, S.P. O'Neal, K.M. Figueroa, S. Hunter, L. Ahle, P.A. Thelin, T. Stefanik, J. Kindem, Development of transparent ceramic Ce-doped gadolinium garnet gamma spectrometers in: Proceedings of the Nuclear Science Symposium Conference Record (NSS/MIC), 2012, p.1692.

[32] L.A. Boatner, J.O. Ramey, J.A. Kolopus, R. Hawrami, W.M. Higgins, E. van Loef, J. Glodo, K.S. Shah, E. Rowe, P. Bhattacharya, E. Tupitsyn, M. Groza, A. Burger, N.J. Cherepy, S.A. Payne, Journal of Crystal Growth 379 (1) (2013) 63.
[33] P.R. Beck, N.J. Cherepy, S.A. Payne, E.L. Swanberg, K.E. Nelson, P.A. Thelin, S.E. Fisher, S. Hunter, B.M. Wihl, K.S. Shah, R. Hawrami, A. Burger, L.A. Boatner, M. Momayezi, K.T. Stevens, M.H. Randles, D. Solodovnikov, Strontium iodide instrument development for gamma spectroscopy and radioisotope identification in: Proceedings of the SPIE Optical Engineering Applications, 2014, p. 92130N.
[34] N.J. Cherepy, Z.M. Seeley, S.A. Payne, P.R. Beck, S. Hunter, L. Ahle, S.E. Fisher, C. Melcher, H. Wei, T. Stefanik, Y.-S. Chung, J. Kindem, High energy resolution with transparent ceramic garnet scintillators in: Proceedings of the SPIE Optical Engineering Applications, 2014, p. 921302.
[35] ⟨http://www.crystals.saint-gobain.com/Scintillation_Materials.aspx⟩.
[36] S. Riboldi, F. Camera, N. Blasi, S. Brambilla, C. Boiano, F.C.L. Crespi, A. Giaz, B. Million, R. Nicolini, L. Pellegri, O. Wieland, Active voltage divider for improved estimation of interacting radiation energy with photomultiplier tubes coupled to high light yield scintillators in: Proceedings of the Nuclear Science Symposium Conference Record (NSS/MIC), 2011, p. 776.
[37] J.G. Rogers, M.S. Andreaco, C. Moisan, I.M. Thorson, Nuclear Instruments and Method in Physics Research Section A 413 (2–3) (1998) 249.
[38] ⟨http://www.wolfmet.com/documents⟩.